Determining Surface Solar Absorption from Broadband Satellite Measurements for Clear Skies: Comparison with Surface Measurements

ROBERT D. CESS

Institute for Terrestrial and Planetary Atmospheres, State University of New York, Stony Brook, New York

ELLSWORTH G. DUTTON AND JOHN J. DELUISI

Climate Monitoring and Diagnostics Laboratory, Environmental Research Laboratories/NOAA, Boulder, Colorado

FENG JIANG

Institute for Terrestrial and Planetary Atmospheres, State University of New York, Stony Brook, New York

(Manuscript received 14 February 1990, in final form 21 August 1990)

ABSTRACT

Two separate datasets both of which provide measurements of net downward shortwave radiation have been combined, so as to provide a means of critically examining methods for transferring satellite measurements to the surface. This is further facilitated through interfacing the two datasets with an atmospheric shortwave-radiation model. One dataset comprises near-surface measurements made at the Boulder Atmospheric Observatory Tower while the other consists of collocated satellite pixel measurements from the Earth Radiation Budget Experiment.

This study amplifies previous suggestions that surface-shortwave absorption is a more meaningful quantity, for climate studies, than is surface insolation. The former should not, however, be evaluated from the latter through use of a surface albedo, since surface albedo is not solely a surface property nor can it easily be evaluated from satellite measurements. It is further demonstrated that a direct evaluation of surface shortwave absorption can be more accurately obtained from satellite measurements than can surface insolation. Specifically, a linear slope-offset relationship exists between surface and surface-atmosphere shortwave absorption, and an algorithm is suggested for transferring satellite shortwave measurements to surface-shortwave absorption. The present study is directed solely at clear-sky conditions because the clear-sky top-to-surface transfer serves as a necessary prerequisite towards treating both clear and overcast conditions.

1. Introduction

The availability of data from the Earth Radiation Budget Experiment (ERBE) has provided unique insights into the radiative exchange processes of the earth's climate system (Ramanathan et al. 1989). By separately averaging clear-sky, top-of-the-atmosphere (TOA) radiative flux measurements, the ERBE provides information concerning the radiative impact of clouds upon climate. There is a critical need to enhance the knowledge of cloud–climate interactions, since Cess et al. (1989) have recently demonstrated that a roughly threefold disagreement in one measure of climate sensitivity exists among 14 atmospheric general circulation models and this was caused by intermodel differences in cloud feedback. Although general circulation models are the most comprehensive numerical climate models for the purpose of projecting climate change due to increasing concentrations of greenhouse gases, cloud–climate interactions, as simulated by these models, must be improved if they are ultimately to be used as reliable climate predictors.

While the ERBE constitutes an important step towards providing cloud–climate information, a comparable surface radiation budget dataset would allow the radiative impact of clouds to be separated into surface and atmospheric contributions. Such information would greatly improve the knowledge of how clouds influence the climate system. Although there is currently considerable effort being directed at ways of implementing surface radiation budget determinations, the problem is a rather formidable one. Radiation measurements made at the surface lack global coverage and are primarily useful in providing ground truth for satellite observations and regional climatological data. Satellite measurements, of course, refer to the TOA, and procedures for transferring such measurements to the surface must be carefully designed and examined.

Corresponding author address: Dr. Robert D. Cess, Institute for Terrestrial and Planetary Atmospheres, State University of New York, Stony Brook, NY 11794-2300.

The purpose of this paper is to address one aspect of the surface radiation budget, namely shortwave (SW) radiation for clear-sky conditions. Specifically, surface measurements are combined with collocated satellite measurements in order to critically examine methods for transferring satellite TOA measurements to the surface, and to understand the physical processes that govern such a transfer. To accomplish this, near-surface downwelling and upwelling (and, thus, net) SW radiation as measured at the top of the Boulder Atmospheric Observatory (BAO) 300-m tower are employed together with collocated ERBE pixel measurements.

2. TOA to surface transfer

Schmetz (1989) summarizes current procedures for estimating surface SW radiation. For the most part, these refer to surface insolation, and there are basically two approaches. One refers to statistical methods in which surface insolation is correlated with satellite TOA SW measurements. As emphasized by Schmetz (1989), a drawback to this approach is that the regression coefficients may be geographically dependent; this point will be amplified shortly. The second approach is the use of physical methods, in which the surface insolation is evaluated from a SW atmospheric radiation model, utilizing input data such as atmospheric water vapor abundance and cloud optical depths or reflectances. An obvious shortcoming here is that a radiometric "dataset" is generated without recourse to radiometric measurements (unless one counts the solar constant).

There are various uses for a SW radiation budget dataset. Some applications require surface insolation, but with respect to understanding climate it is the net SW at the surface (surface SW absorption) that is the relevant quantity. The only way to obtain this from surface insolation data is to employ a surface albedo, but this approach contains substantial problems (e.g., Cess and Vulis 1989), which will be amplified in section 5.

As suggested by Ramanathan (1986) and as further examined by Cess and Vulis (1989), there appears to be an attractively simple linear relationship between surface SW absorption and surface-atmosphere SW absorption; i.e., between the net downward SW fluxes at the TOA and at the surface. This is demonstrated for three surface categories as is shown in Fig. 1 for clear skies and in the absence of tropospheric aerosols. These results are taken from Cess and Vulis (1989) and were obtained from an atmospheric SW radiation model. Here the flux variation, in proceeding from right to left, corresponds to an increase in solar zenith angle. As Cess and Vulis discuss, if the atmosphere contained only conservative scatters, then there would be a one-to-one relationship between the surface and the TOA net fluxes, irrespective of surface albedo. This is because the surface albedo equally affects the TOA and surface

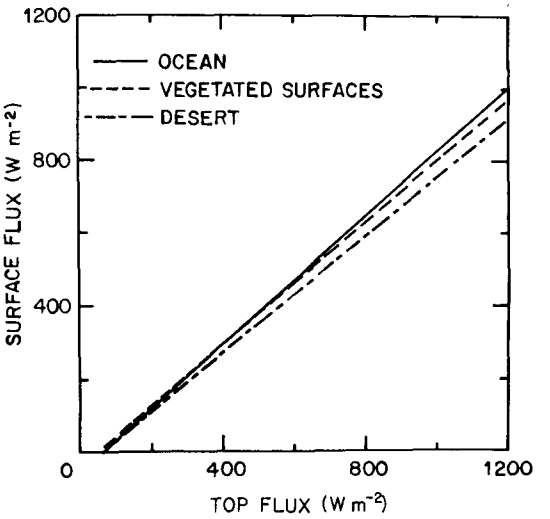

FIG. 1. Comparison of model-generated linear regressions of net-surface flux as a function of TOA flux (from Cess and Vulis 1989).

fluxes. Consider next the addition of saturated (i.e., opaque) absorbers, which in fact is the case for solar absorption throughout much of the water vapor spectrum. The addition of this absorption does not introduce a surface albedo dependence, since there is no insolation (and hence no surface reflection) in these spectral intervals. This saturated absorption will, of course, reduce the surface SW flux relative to that at the TOA.

A dependence upon surface albedo arises only through the inclusion of weak absorbers and with reference to Fig. 1 these include weak water vapor absorption and ozone absorption. The reason for this dependence is that in progressing to brighter surfaces (e.g., ocean to vegetated surfaces to desert in Fig. 1) the weak absorption is enhanced due to increased reflection of SW radiation by the surface. As seen in Fig. 1, however, this effect is quite small, and as discussed by Cess and Vulis (1989), vegetated surfaces may be considered as a single-surface classification irrespective of vegetation type. The surface classifications of Fig. 1 coincide with those of the ERBE.

Cess and Vulis (1989, their Fig. 18) additionally incorporated background tropospheric aerosols consisting of maritime aerosols over the ocean, continental aerosols over vegetated surfaces, and desert aerosols over deserts. Since maritime aerosols are nearly conservative scatterers, they have virtually no impact upon the ocean results. Modest absorption by continental aerosols over vegetated land produced a slight slope decrease. This was more pronounced over deserts because desert aerosols have a greater optical depth.

The important conclusion that may be drawn from Fig. 1, and with restriction to clear-sky conditions, is that there appears to be a simple slope-offset relationship between the net downward SW fluxes at the TOA

and at the surface. Because these coincide with the ERBE surface classifications suggests that a rather simple algorithm might apply for the purpose of transferring ERBE net SW measurements to net SW fluxes at the surface, as will be shown shortly.

3. Atmospheric radiation model

An atmospheric SW radiation model is employed as a vehicle to both interpret and understand the combined TOA and surface measurements of net SW radiation. This model is a five-layer (equally spaced pressure levels) delta Eddington model similar to that employed by Cess and Vulis (1989), but with modifications. The spectral resolution, Rayleigh optical depths (referenced to a surface pressure of 1013 mb), and absorber optical depths are summarized in Table 1. In that the spectral resolution in Table 1 is insufficient to account for the strong wavelength dependence of Rayleight scattering, the values of τ_R were determined through further subdivision of each interval and then evaluating a mean τ_R which reproduced the atmospheric Rayleigh reflectance for that interval.

Ozone is assumed to absorb all solar radiation at wavelengths less than 0.3 μm. The UV and visible (0.5–0.7 μm) optical depths in Table 1 were obtained by fitting the exponential attenuation law to the ozone absorption parameterizations of Lacis and Hansen (1974), renormalized from their full solar spectrum to the wavelength intervals of Table 1. Ozone absorption is restricted to the model's top layer. The H_2O absorption optical depths for the 0.72- and 0.81-μm bands were obtained from exponential fits to line-by-line absorptance calculations. For absorption at wavelengths greater than 0.9 μm, the latter five terms of the six-term exponential sum fit presented by Somerville et al. (1974) were used. The first term in this fit represents H_2O absorption at wavelengths less than 0.9 μm, and this is already included in the present model. The model utilizes total-column precipitable water as an input parameter with the vertical water-vapor profile being an average of the McClatchey et al. (1971) midlatitude winter and summer profiles. The model output is quite insensitive as to this choice.

TABLE 1. Spectral resolution, Rayleigh optical depth τ_R, and absorber optical depths τ. Here, OZ and WA represent the ozone and water vapor column abundances (cm).

Spectral interval (μm)	τ_R	τ
0.30–0.35	0.830	0.13 × OZ
0.35–0.40	0.465	—
0.40–0.50	0.226	—
0.50–0.60	0.099	0.085 × OZ
0.60–0.70	0.050	0.085 × OZ
0.70–0.80	0.028	0.025 × WA
0.80–0.90	0.017	0.033 × WA
>0.90	—	Lacis and Hansen (1974)

Tropospheric aerosols are incorporated within the model's lowest layer. For the present application, aerosol optical properties have been interpolated in wavelength from those summarized for continental aerosols by Deepak and Gerber (1983); they are listed in Table 2.

The savannah surface-albedo model of Vulis and Cess (1989) is adopted, which lies between their pasture land and bog models. As Cess and Vulis (1989) demonstrated and as has been previously emphasized, the TOA to surface SW flux transfer for vegetated surfaces is essentially invariant to vegetation type, a point that will be confirmed through use of the TOA and surface SW flux measurements. As a consequence of alternate-year farming, about 20%–30% of the area viewed from the top of the tower is actually bare soil.

The tower measurements of net-SW radiation are at a pressure that is 30 mb less than the 835-mb surface pressure. Nominally the model employs five equally spaced pressure levels, so that for an 835-mb surface each layer is 167 mb thick. To facilitate interpretation of the measurements, however, the vertical resolution of the model was modified, so that the thickness of the lowest layer was 30 mb, while that of the next layer was 304 mb. The three remaining layers retain their 167 mb thickness. Because of this change in vertical resolution relative to the nominal model, tropospheric aerosols were excluded from this example.

Illustrated in Fig. 2 is the relationship between the 805 mb net flux (tower top) and the TOA flux, for 2 cm of precipitable water above the 805-mb level, 0.3 cm of ozone, and both 0.5 cm and 0 cm of precipitable water below the 805-mb level. These simulations were performed by varying μ = cos(solar zenith angle) from $\mu = 1.0$ (overhead sun) to $\mu = 0.2$ with a $\Delta\mu = -0.04$ progression in going from right-to-left. For clarity, only alternate model points are shown; $\mu = 1, 0.92, \cdots$ for the filled circles; and $\mu = 0.96, 0.88, \cdots$ for the open circles. Although these alternate model points exhibit a slightly unequal spacing, they have virtually the same linear fit. For the data that will be employed, the precipitable water below 805 mb is typically 0.25 cm or less, so that in the following the 805-mb measurements will be referred to as "surface measurements" while adopting an 805-mb "surface pressure" within the model together with measured precipitable water above the 805-mb level.

4. Datasets

In addition to the ERBE satellite measurements and the BAO tower measurements, precipitable water and aerosol optical depths are also utilized which were measured at locations near the tower. Each of these four datasets is described in the following subsections.

TABLE 2. Optical properties of the continental aerosol model where g denotes the asymmetry factor, ω is the single-scattering albedo, and τ is the aerosol optical depth with τ_{vis} that at 0.55 μm.

Spectral interval (μm)	g	ω	τ/τ_{vis}
0.30–0.35	0.657	0.882	1.72
0.35–0.40	0.645	0.911	1.51
0.40–0.50	0.637	0.919	1.24
0.50–0.60	0.636	0.896	1.00
0.60–0.70	0.636	0.868	0.81
0.70–0.80	0.635	0.855	0.70
0.80–0.90	0.630	0.855	0.61
>0.90	0.630	0.801	0.45

a. BAO tower measurements

Since December 1985, continuous surface-based radiation measurements have been obtained from radiometers mounted on top of the 300 m BAO tower. The tower is located at 40.048°N, 105.008°W, about 25 km north of Denver. The tower is surrounded by dry-plains agricultural land nominally typical of the adjoining several hundred square kilometers to the east, the Rocky Mountains beginning 25 km to the west, and the Denver metropolitan area beginning 20 km to the south. The tower was originally designed and built for boundary-layer research (Kaimal and Gaynor 1983).

The upwelling and downwelling SW irradiances are obtained with leveled downfacing and upfacing hemispheric field-of-view Eppley pyranometers. The upfacing instrument is mounted on the highest point of the tower while the downfacing instrument is mounted on a 3-m boom extending out from the tower's top level. The tower is blocked from the field-of-view of the downfacing pyranometer by an optically black plate which is accounted for in the applied calibration of the instrument.

The pyranometers were calibrated at the NOAA Solar Radiation Facility relative to an active-cavity radiometer which regularly participates in the International Pyrheliometer Comparison (IPC). The IPC includes many other similar radiometers and is conducted by the WMO in Davos, Switzerland. The cosine response error of the upfacing pyranometer was determined to be less than 5 W m^{-2} at any zenith angle. Corrections for the cosine response error are not applied to the data reported here. The downfacing pyranometer was compared to the upfacing instrument in side-by-side comparisons with diffuse light before installation on the tower. The correction for the black plate used to block the tower was theoretically derived to be 11.8 percent and observationally determined to be 12.4 percent. Periodic calibration comparisons are made with standard instruments temporarily placed on the tower. An uncertainty analysis of instrument performance and calibration procedure suggest a measurement accuracy of better than the largest part of ±2 percent or ±7 W m^{-2} for the downwelling and ±2 percent for the upwelling. The possible error in the net SW values used in this paper is further minimized because the cross-reference calibration between the two instruments reduces any bias in the absolute calibration.

Routine measurements consist of one-hour averages of raw voltages sampled every five seconds. The data are processed as one-hour averages (in W m^{-2}) by multiplying the raw voltage average by the linear calibration factor. The results are objectively and manually examined for unreasonable data. Occasional invalid data are acquired because of maintenance, snow, and/or ice accumulation on the upfacing instrument or other causes. Data determined to be invalid are excluded.

b. Precipitable water

Precipitable water amounts used in this study were calculated from routine Denver National Weather Service (NWS) noon and midnight UTC radiosonde data. The NWS balloons are launched 25 km south of the BAO tower. Temperature and relative humidity data from all reported levels are acquired in "near"-real time directly from the Denver NWS office and maintained as a computer database at NOAA/ERL in Boulder. Standard equations are used to calculate the precipitable water amount from the surface to the top of the sounding. The precipitable water integration was also performed from 30 mb above the surface (approximate height of the tower) to the top of the sounding. As previously mentioned, this is the water vapor amount that will be used in the present study. Although this requires interpolation between levels of the sounding, the procedure is reasonable since there was typically

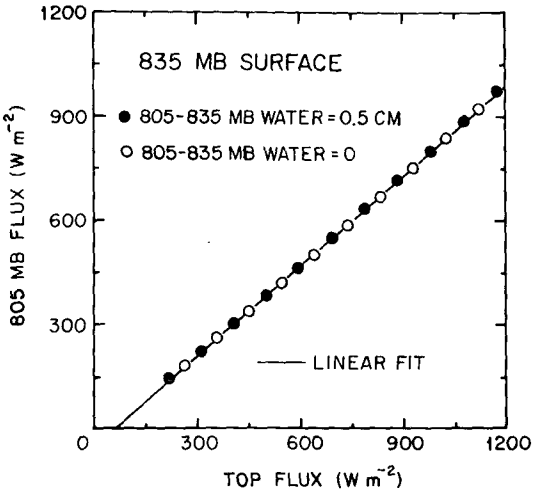

FIG. 2. Model-generated 805-mb flux as a function of the TOA flux for a surface pressure of 835 mb. Above 805 mb the precipitable water abundance is 2 cm, and the ozone abundance is 0.3 cm. There are both 0.5 cm and 0 cm of precipitable water below 805 mb. Only alternate model points are shown (see text).

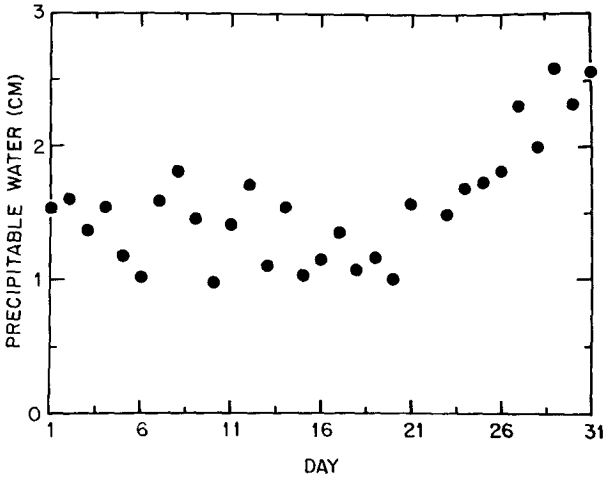

FIG. 3. Daily mean precipitable water for July 1987.

at least one significant level reported between the surface and the top of the tower. The percentage of the total-column precipitable water present between the surface and the top of the tower varies from 5 percent in winter to 11 percent in summer based on a 16-year average. As discussed in section 4d, the present study is restricted to July 1987. Total-column precipitable water above the 820-mb level is shown in Fig. 3 for this month; these values refer to 0000 and 1200 UTC averages.

c. Aerosol optical depth

The aerosol optical depth data used in this study are derived from routine spectral (0.5 μm in the present case) optical depth measurements made for NOAA/Geophysical Monitoring for Climatic Change (GMCC) in Boulder, 20 km west of the tower. These observations are performed manually with sunphotometers under clear-sky conditions several times a day. The long-term stability of the sunphotometer calibration is maintained through frequent high-altitude calibration by the Langley method and comparison with standard instruments whose calibration is specially maintained. Daytime-average optical depths are shown in Fig. 4 for July 1987; missing data refer to weekends and the Fourth of July holiday.

d. ERBE satellite data

At the time this study was conducted, there were three months of processed ERBE data that coincided with BAO tower data: January and October 1986 and July 1987. Neither the January nor October data proved to be particularly useful because the main thrust of the present study is directed towards clear-sky conditions, and there was a predominance of broken clouds during these two months. In addition, anthropogenic haze was present on many days when the skies were clear. These problems were largely absent during July 1987, the month chosen for this study, and the extended July daytime length additionally provided a greater number of collocated SW measurements.

An overview of the ERBE is given elsewhere (ERBE Science Team 1986). The data used here are those provided by the SW cross-track scanner on the Earth Radiation Budget Satellite (ERBS) whose orbit has a 57 degree inclination angle relative to the equator. Because of this orbit, the scanner views the vicinity of the tower as many as three times a day for some days, while more typically it is one or two times and on some days not at all. The scanner-measured radiances are converted to irradiances (fluxes) within the ERBE data reduction system through use of bidirectional models, which perform the conversion as a function of solar zenith angle, viewing zenith angle, and relative azimuth angle.

The scanner pixel is nearly circular in shape with a nadir diameter of roughly 35 km, which is considerably larger than the area viewed by the downfacing tower pyranometer. Thus, for the ERBE and tower measurements to be compatible, the terrain surrounding the tower must be representative of that below the tower. To demonstrate that this is largely the case, Figs. 5 and 6 are maps of the TOA albedo as determined from individual pixel measurements in the vicinity of the tower; the geographic size of these maps is roughly 100 km longitude $\times$ 130 km latitude. The albedos are designated by circled numbers; these circles denote only the pixel locations and are not representative of the pixel size. That these albedos are larger on 25 July (Fig. 6 versus Fig. 5) is due to different solar zenith angles at the times of the satellite overpass.

Note the lower albedos to the west of the tower, as is consistent with the existence of the foothills of the Rocky Mountains. To the east, however, there is significant uniformity and this prevails well beyond the range of these figures. To avoid contamination by the

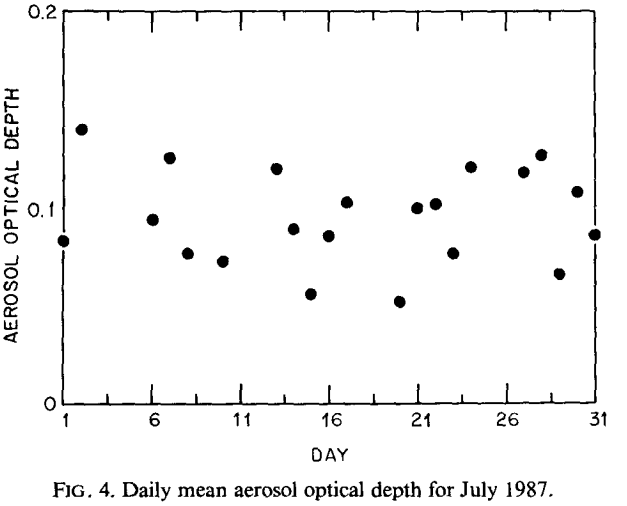

FIG. 4. Daily mean aerosol optical depth for July 1987.

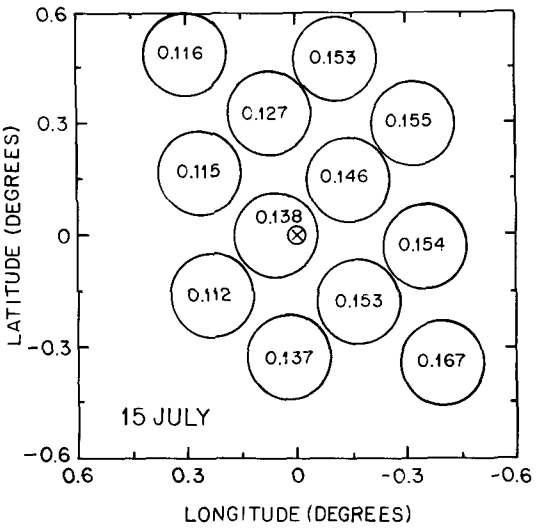

FIG. 5. TOA albedos in the vicinity of the tower for 15 July 1987. Longitude and latitude are relative to the tower location that is designated by the circled cross.

city of Boulder and the foothills, as well as the Denver metropolitan area to the south of the tower, the procedure is to select pixels to the east of the tower. Thus, for example, the 0.154 and 0.204 albedo pixels have been respectively selected in Figs. 5 and 6.

5. The surface albedo

As have been previously discussed, most efforts at determining the SW surface-radiation budget are concerned with surface insolation, whereas a more useful quantity for climate studies is the net SW flux at the surface. The only way surface insolation can be converted to net-surface SW is through use of a surface albedo, but as emphasized by Cess and Vulis (1989) inferences of the surface albedo can involve substantial uncertainties. This is an important issue and, consequently, both the atmospheric radiation model and the tower data will be employed to further demonstrate uncertainties and difficulties in estimating the surface albedo.

The first issue concerns use of narrowband TOA measurements to evaluate a narrowband surface albedo (e.g., Sellers et al. 1988). This can probably be accomplished with reasonable accuracy; the problem, as demonstrated by Cess and Vulis (1989) is the next step involving conversion of the narrowband surface albedo to a broadband quantity. To reinforce this point, the spectral resolution of the atmospheric radiation model has been increased to accommodate an approximation to the GOES filter function (Rossow et al. 1987). The radiation model was then used to evaluate both the broadband and narrowband (GOES) surface albedos. Broadband versus narrowband calculations are summarized in Fig. 7 for several vegetation types for which the spectral surface albedos were obtained from Bowker et al. (1985). These results suggest that there is neither a simple nor accurate way of performing a narrowband-to-broadband surface albedo conversion for vegetated surfaces.

An alternate procedure for estimating broadband surface albedos from satellite measurements makes use of linear fits, derived from simulations with atmospheric radiation models of the planetary albedo as a function of surface albedo (e.g., Nack and Curran 1978; Preuss and Geleyn 1980; Chen and Ohring 1984; Pinker 1985). Gutman et al. (1989), for example, have employed the regression of Chen and Ohring (1984) in their satellite estimates of surface albedo for the United States Great Plains. Illustrated in Fig. 8, for the same conditions and surface types as in Fig. 7, are model-derived surface versus planetary broadband albedos. The Chen and Ohring (1984) regression fit, which assumes a wavelength-invariant surface albedo, is also shown for comparative purposes. Clearly, this type of conversion would seem to depend upon vegetation type; i.e., upon the wavelength dependence of the surface albedo.

Further insights are provided by the July tower data. If $Q(\lambda, \mu)$ is the surface insolation, while $\alpha_s(\lambda, \mu)$ is the spectral–directional surface albedo with λ representing wavelength, then the broadband surface albedo $\bar{\alpha}_s(\mu)$ is defined by

$$\bar{\alpha}_s(\mu) = \int_0^\infty \alpha_s(\lambda, \mu) Q(\lambda, \mu) d\lambda \Big/ \int_0^\infty Q(\lambda, \mu) d\lambda. \quad (1)$$

As emphasized by Sparrow and Cess (1966), (1) reveals that $\bar{\alpha}_s(\mu)$ depends on two factors. First, there is the reflection characteristic of the surface as embodied in $\alpha_s(\lambda, \mu)$; second, there is the nature of the incident radiation as embodied in $Q_s(\lambda, \mu)$, and this in turn is

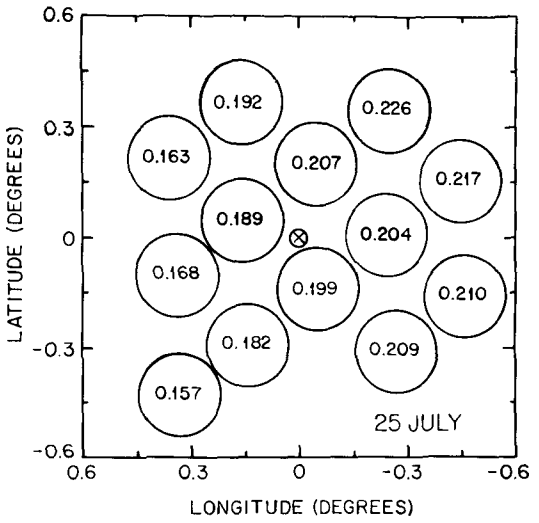

FIG. 6. As in Fig. 5, but for 25 July 1987.

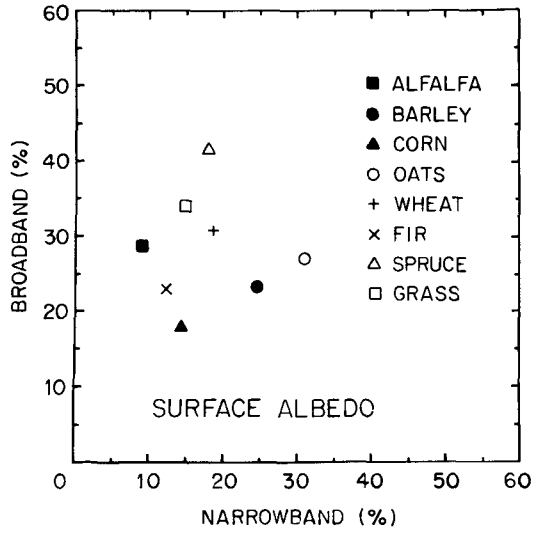

FIG. 7. Comparison of model-generated broadband versus narrowband surface albedos for $\cos(SZA) = 0.5$, where SZA is the solar zenith angle.

dependent upon atmospheric composition. Therefore, the broadband surface albedo cannot be regarded as being solely a property of the surface since it is also a function of atmospheric composition. For example, since $\alpha_s(\lambda, \mu)$ generally increases with λ for vegetated surfaces, then a decrease in atmospheric water vapor content will increase $Q(\lambda, \mu)$ in the near infrared, which will in turn increase $\bar{\alpha}_s(\mu)$, as was demonstrated by Cess and Vulis (1989).

A comparison of early morning (0600–0700 local time) and midmorning (1000–1100) surface albedos (Fig. 9), as measured for the area underlying the tower,

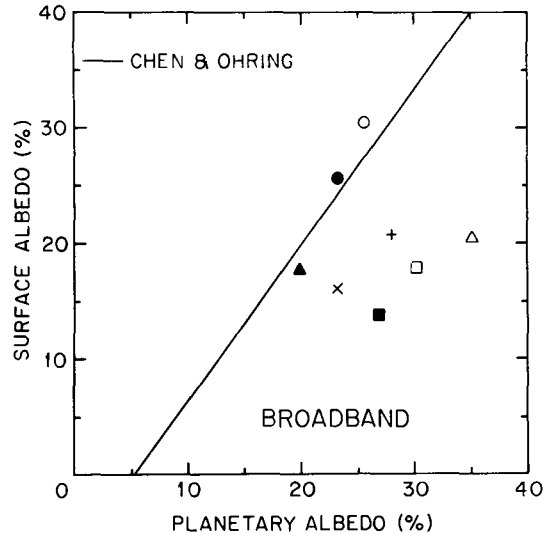

FIG. 8. Comparison of model-generated surface versus planetary albedos for $\cos(SZA) = 0.5$. The solid line is from Chen and Ohring (1984). The surface vegetation types are the same as in Fig. 7.

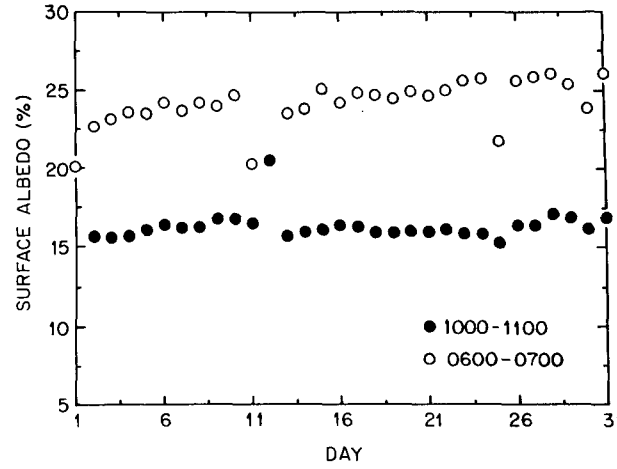

FIG. 9. Tower measurements of early morning (0600–0700) and late morning (1000–1100) surface albedos for July 1987.

reveals several features. The enhancement of the early morning albedo is, of course, caused by the dependence upon solar zenith angle. For the most part the results in Fig. 9 refer to clear skies. Notable exceptions occur for 1, 11, 12, 25, and 30 July. On 11 July the tower measurements indicate dense overcast conditions for 0600–0700 but clear skies for 1000–1100. The surface-albedo measurements are consistent with this since the presence of a dense cloud will convert $Q(\lambda, \mu)$ in (1) from primarily direct beam (clear skies) to primarily diffuse radiation. The latter results in a smaller "effective" solar zenith angle (relative to 0600–0700) and thus a smaller albedo (Fig. 9). Just the reverse occurs for 12 July, when there is dense cloud cover for 1000–1100 because here the effective diffuse solar zenith angle is greater than that for 1000–1100. The lack of a 0600–0700 value is because early morning cloud cover produced nearly total solar attenuation for that hour. There is substantial interannual variability, as is demonstrated in Fig. 10 for the late afternoon when there is often convective activity in July with the ensuing impact of broken clouds upon $Q(\lambda, \mu)$ in (1).

The point of this section is that the broadband surface albedo is not a surface property, nor is it a quantity that can easily be evaluated from satellite measurements using either narrowband or broadband instruments. Because of this, any procedure for inferring the net surface SW flux should be one that bypasses the need and use of surface albedo information.

6. Clear-sky comparisons

For July 1987, 31 clear-sky ERBE pixels were collocated with the BAO Tower. The corresponding net-downward SW flux measurements made at the tower are shown in Fig. 11. These are hourly mean measurements, and they are for the hour bins within which the ERBE data are contained. These hourly means are

the only available tower data since the original purpose of the tower measurements was to provide average radiation budget information. The linear dependence upon cos(*SZA*), however, allows the following procedure for obtaining temporal collocation of the ERBE and tower data. By utilizing the slope of the linear fit in Fig. 11, each of the tower measurements has been relocated so as to coincide with the ERBE cos(*SZA*) values.

Illustrated in Fig. 12 is a plot of the temporally relocated tower data versus the ERBE TOA data. The standard error of 19 W m^{-2} (or 2.9%) is quite modest considering that two different datasets have been combined. Bear in mind, however, that this standard error includes day-to-day variability in both atmospheric water vapor and aerosol optical depth, and it appears that much of the variance in Fig. 12 is explained by this variability. For example, the atmospheric SW radiation model produces a 14 W m^{-2} standard error when daily mean water and aerosol measurements (for the same days as the tower/ERBE measurements) are employed as input for the model. Here and in the following, a climatological ozone abundance of 0.3 cm is adopted.

Conversely, employing monthly mean water and aerosol data (WA = 1.55 cm and $\tau = 0.095$), the model produces virtually the same linear fit (Fig. 13) as does the use of daily data (not shown). The significance of this is that if one is interested only in monthly mean TOA-to-surface conversion, then this can be achieved through use of monthly mean water data and only rudimentary aerosol optical depth information, since most of the 14 W m^{-2} standard error in the model simulation is due to water vapor variability. The standard error of 2 W m^{-2} in Fig. 13 is a sole consequence of the linear fit.

Illustrated in Fig. 14 is the same scatter plot as in Fig. 12, but here compared against the linear fit to the monthly mean model of Fig. 13. The mean error of 3 W m^{-2} (i.e., 0.5%) is rather remarkable. In that the model is being compared to two separate datasets, the possibility exists that a bias in one of the two datasets is being compensated for by a bias in the model. The likelihood of this being the case is significantly diminished in that the same agreement (0.5 percent) was found to exist between the tower insolation measurements and the model. For whatever reasons the model seems to be quite accurate while this consistency with both tower/ERBE and tower data speaks well for the quality of the two datasets.

There are several other data-to-model comparisons that provide valuable insights into the TOA to surface transfer. For example, comparing the model to tower measurements of the net-downward SW flux at the

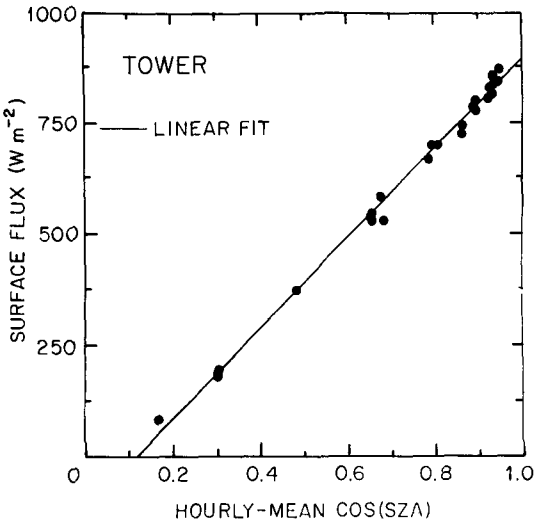

FIG. 11. Tower net-surface flux as a function of the hourly mean cosine of the solar zenith angle.

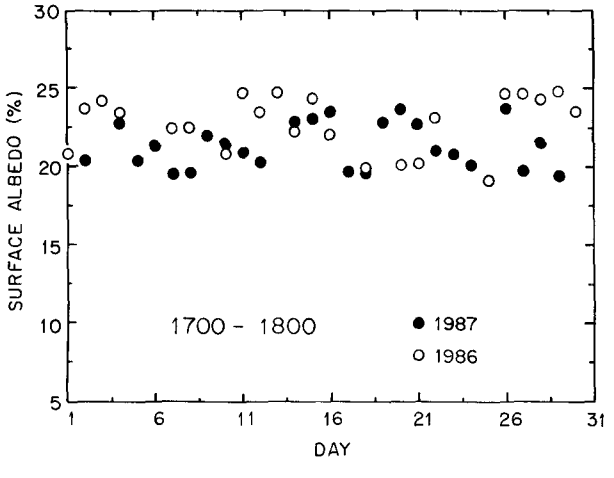

FIG. 10. Tower measurements of late afternoon (1700–1800) surface albedos for July 1986 and 1987.

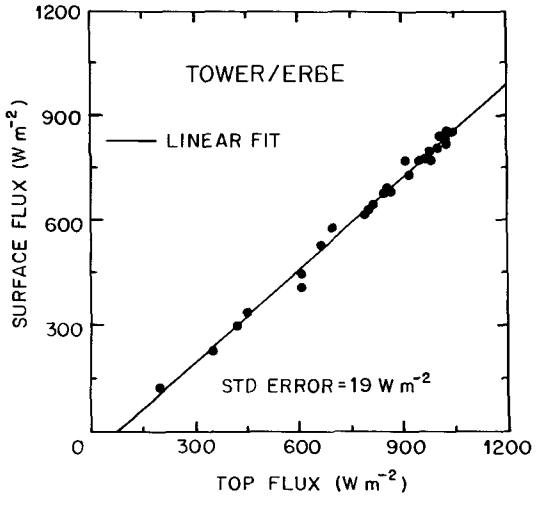

FIG. 12. Tower surface flux as a function of the ERBE TOA flux.

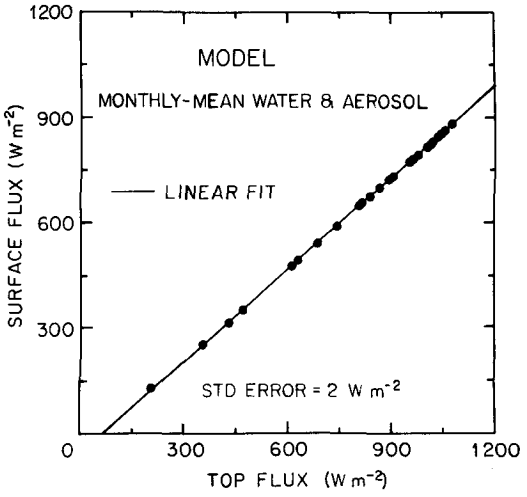

FIG. 13. Model-generated net-surface flux as a function of the net-TOA flux employing monthly mean water abundance and aerosol optical depth.

surface produces a mean model error of 30 W m^{-2}, as opposed to the 3 W m^{-2} mean error in Fig. 14. Conversely, comparing the model to the ERBE TOA measurements results in a mean-model error of 28 W m^{-2}. Thus, the extraordinary data-to-model agreement in Fig. 14 is actually the result of compensatory TOA and surface errors in the model. But unlike most compensatory error situations, this case helps to more fully understand the underlying principles concerning the TOA-to-surface transfer in Fig. 14.

The fact that the model produces significant individual errors in the net-SW TOA and surface fluxes is easily understood. Within the SW atmospheric radiation model, a surface albedo model has been incorporated, which has been derived from Kriebel's (1977) savannah measurements (Vulis and Cess 1989), and this albedo model is not representative of the brighter dry-plains agricultural land in the vicinity of the BAO Tower. Thus, the individual TOA and surface errors (28 and 30 W m^{-2}, respectively) are caused by this discrepancy in surface albedo.

But this compensatory behavior is, in fact, consistent with the model. For example, as emphasized by Cess and Vulis (1989), the TOA-to-surface net-SW transfer is quite invariant to the choice of vegetation type (i.e., choice of vegetation surface albedo). Thus, when replacing one vegetation type by another within the model, the resulting change in net-SW surface radiation must be compensated for by a similar change at the TOA. In this context, the near-compensatory 30 and 28 W m^{-2} errors actually serve to validate this model interpretation.

This compensatory behavior also helps one to understand potential pitfalls associated with conventional statistical methods in which surface insolation measurements are correlated with collocated satellite measurements. Illustrated in Fig. 15 are surface insolation measurements plotted against the TOA net-SW measurements. While the two datasets exhibit a near-linear correlation, here the model produces a negative 27 W m^{-2} mean error, which is easily understood. The inappropriate surface albedo within the model will have little impact upon surface insolation, but as previously demonstrated it produces a mean overestimate of 28 W m^{-2} in the TOA flux that in turn results in the similar, but negative, error in Fig. 15.

This raises a very important issue concerning statistical methods. These comparisons have shown us that correlating surface insolation measurements with TOA satellite measurements should result in regression coefficients that depend upon surface albedo and hence upon geographical domain. This same constraint, at least with restriction to vegetated domains, does not appear to apply to net-SW TOA-to-surface correlations. Thus, it would seem that the net-surface flux can be more accurately inferred from satellite measurements than can the surface insolation.

7. A retrieval algorithm

The combined ERBE and BAO tower data have served to validate the atmospheric radiation model as a vehicle for transferring net SW measurements from the TOA to the surface for clear-sky conditions. In principle, this validation is restricted to the tower environment and thus to a single-surface category. The model and the measurements, however, are consistent with the suggestion that differences in vegetation type have little impact upon the TOA to surface net-SW transfer, while the model results of Fig. 1 show that, in general, the surface category, such as ocean versus vegetated land has only a secondary impact.

A more reasonable concern is that the tower data

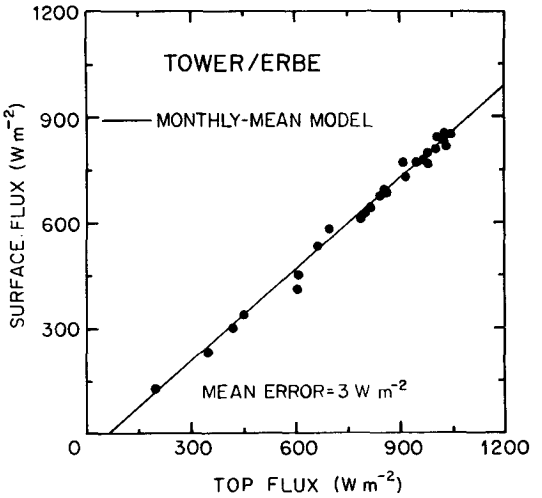

FIG. 14. Model and tower/ERBE comparison of the top-to-surface flux transfer.

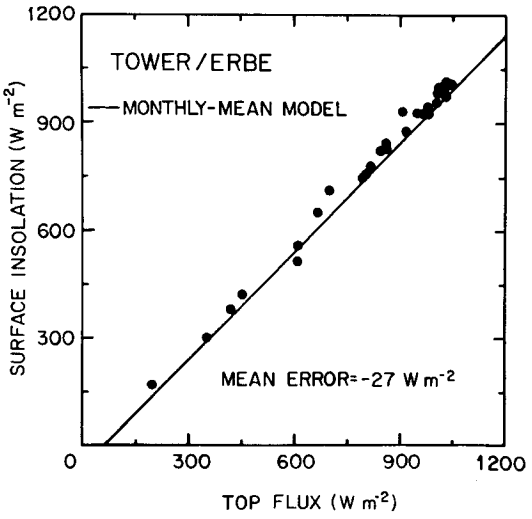

FIG. 15. Model and tower/ERBE comparison of TOA flux to surface insolation transfer.

respond to variations of water vapor abundance (Fig. 5), and it obviously would be beneficial if additional near-surface net SW measurements were available which spanned a greater range of geographical domains and water vapor abundances. This is not the case; other near-surface net-SW measurements were available ERBE pixel measurements are currently unknown to this particular study. It will thus be tentatively and necessarily assumed that the tower/ERBE validation applies to a broader range of conditions than is represented by the tower location. This assumption is made for the purpose of illustrating and examining an algorithm approach for transferring to the surface ERBE net-SW measurements.

Consistent with Fig. 1, the slope–offset expression is begun with

$$\mathrm{SURF} = A + B \times \mathrm{TOP}, \qquad (2)$$

where SURF and TOP denote the net-SW flux at the surface and at the TOA. From the SW model, the coefficients A and B are found to depend primarily on the column water vapor abundance (WA); the dependence on aerosol optical depth is much less. This is demonstrated for two surface categories: vegetated land and ocean. For the latter the surface albedo is taken from Briegleb et al. (1986) together with the maritime aerosol model of Deepak and Gerber (1983). This study refrains from considering deserts for two reasons. First, there is considerable variability in surface albedo among deserts, ranging from the bright Saudi saline desert to the darker Gibson desert where red clay compounds are present; it is doubtful that deserts could be combined into a single-surface category. Second, desert aerosols strongly impact the TOA-to-surface transfer (Cess and Vulis 1989), and the optical depth of these aerosols is highly variable in time (d'Almeida 1987) while their optical properties are poorly understood and undoubtedly vary from one desert to another.

Surfaces covered by snow and ice are also excluded since, again, there can be substantial variations in surface albedo for this surface category. For example, the difference in surface albedo between new and aged snow can exceed that for desert versus ocean, and Fig. 1 demonstrates that this could produce a significant uncertainty in a snow/ice retrieval algorithm.

The coefficients A and B in (2) have been evaluated by simultaneously varying μ from 0.2–1.0 and WA from 0.25–10 cm within the radiation model. The dependence on WA is accurately described by the empirical expressions

$$A(\mathrm{W\ m^{-2}}) = -A_0 - A_1 \times \ln[1 + A_2 \times \mathrm{WA(cm)}], \qquad (3)$$

$$B = B_0 - B_1 \times \ln[1 + B_2 \times \mathrm{WA(cm)}], \qquad (4)$$

as is demonstrated in Fig. 16 for vegetated land, $\tau = 0.1$ and OZ = 0.3 cm. The coefficients in these expressions, determined from regression fits, are summarized in Table 3 for several aerosol optical depths.

Although the coefficients in Table 3 were evaluated for a surface pressure of 1013 mb and OZ = 0.3 cm, they are quite insensitive to these choices. This is demonstrated by the sensitivity analyses summarized in Table 4 for vegetated land. Here, mean input data corresponding to the tower location (WA = 1.55 cm and

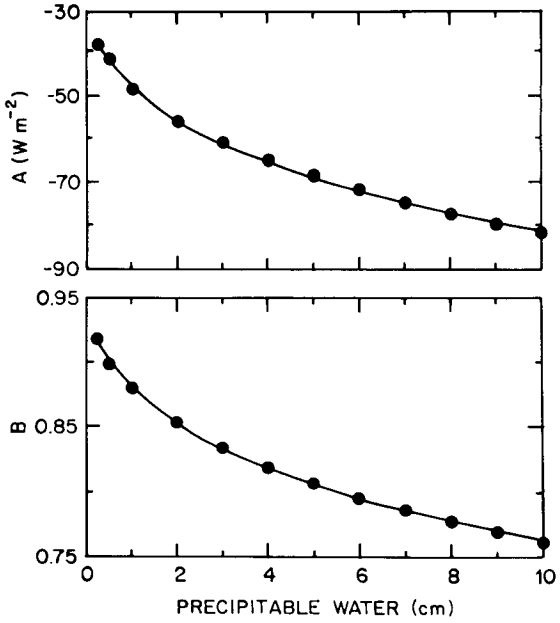

FIG. 16. The coefficients A and B in Eq. (2) as a function of precipitable water. These refer to vegetated land with $\tau = 0.1$ and OZ = 0.3 cm. The filled circles denote model calculations while the solid lines represent Eqs. (3) and (4).

TABLE 3. Algorithm coefficients as a function of aerosol optical depth (τ) and surface type (vegetated land and ocean) for OZ = 0.3.

τ	A_0	A_1	A_2	B_0	B_1	B_2
			Vegetated land			
0	24.44	20.83	0.956	0.9388	0.0671	1.115
0.1	34.45	19.34	1.000	0.9316	0.0676	1.093
0.2	42.53	17.84	1.039	0.9222	0.0681	1.075
			Ocean			
0	28.94	24.21	1.055	0.9539	0.0603	0.911
0.1	30.65	23.26	1.103	0.9529	0.0620	0.905

clear-sky TOP = 834 W m^{-2}) were adopted, and A and B in (2) were evaluated from the μ = 0.2 to 1.0 variation. Note in particular the rather modest impact due to continental aerosols, suggesting that only rudimentary aerosol optical depth information would be required over vegetated land. There is a minimal effect due to maritime aerosols over the ocean, as is obvious by comparing the ocean τ = 0 and τ = 0.1 coefficients in Table 3. This is because the maritime aerosol is nearly a conservative scatterer. These conclusions are more comprehensively demonstrated in Fig. 17.

There are exceptions to the above conclusions, such as areas where desert aerosols are transported over nondesert regions. A specific example is the portion of the Atlantic Ocean located off the west coast of north Africa. On the other hand, it is important to note that stratospheric aerosols will have no influence on (2) because they are essentially conservative scatterers.

The relative invariance of (2) upon vegetation type can be further demonstrated by adopting surface albedo models for pasture land and bog (Cess and Vulis 1989) within the radiation model, in addition to savannah as used in the nominal model. Values of A and B are summarized in Table 5 for these three vegetation types and for monthly mean input quantities that correspond to the combined clear-sky tower/ERBE tower data; clearly there is little dependence upon vegetation albedo. A greater influence exists with respect to the analogous treatment of surface insolation, as would be expected from previous discussion. This is demonstrated in Table 6, where the coefficients C and D refer to

$$\text{INSOL} = C + D \times \text{TOP} \qquad (5)$$

with INSOL denoting surface insolation.

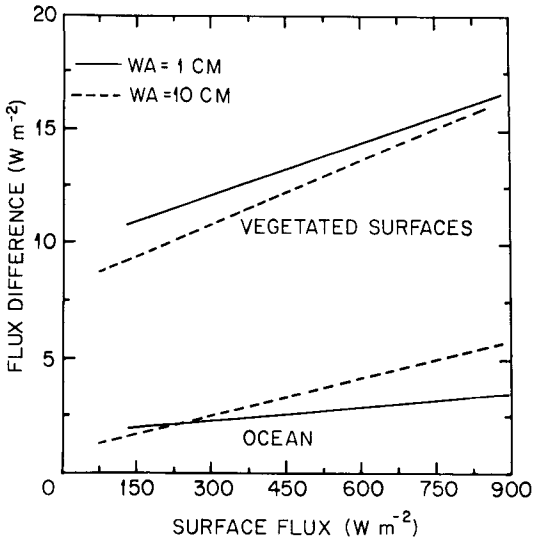

FIG. 17. The surface flux difference, defined as the surface flux for τ = 0 minus that for τ = 0.1, as a function of the surface flux for τ = 0.1. These are for OZ = 0.3 cm.

8. Conclusions

The following conclusions can be drawn from the present study:

- Surface radiation budget efforts should address the needs of those who want to use the data to understand the climate system. In this regard, surface SW absorption is a more meaningful quantity than is surface insolation.
- It would appear that surface SW absorption can be more accurately determined from satellite data than can surface insolation. This is because the TOA to surface net SW transfer is less sensitive to surface albedo

TABLE 4. Sensitivity of net-SW surface flux to input parameters for vegetated land with WA = 1.55 cm and TOP = 834 W m^{-2}. Surface pressure is denoted by P_s.

Change of input parameter	Surface flux difference (W m^{-2})	(Percent)
τ = 0.1 to 0	14.9	2.2
τ = 0.1 to 0.2	−14.7	−2.2
OZ = 0.3 to 0.2 cm	3.8	0.6
OZ = 0.3 to 0.4 cm	−3.7	−0.6
P_s = 1013 to 820 mb	0.9	0.1

TABLE 5. The coefficients A and B (WA = 1.55, τ = 0.095, OZ = 0.3 cm), and the mean error of Eq. (2) relative to the clear-sky tower/ERBE data.

Surface	A (W m^{-2})	B	Mean error (%)
Pasture land	−55.6	0.845	−2.8
Savannah	−53.3	0.865	0
Bog	−58.8	0.876	0.6

TABLE 6. The coefficients C and D (WA = 1.55 cm, τ = 0.095, OZ = 0.3 cm), and the mean error of Eq. (5) relative to the clear-sky tower/ERBE data.

Surface	C (W m^{-2})	D	Mean error (%)
Pasture land	−44.5	1.050	3.7
Savannah	−61.1	0.998	−3.7
Bog	−40.6	0.956	−5.5

than is the analogous conversion of TOA net SW to surface insolation.

- Surface SW absorption (net SW) should not be determined through combining surface insolation estimates with surface albedo estimates. As emphasized both in this study and by Cess and Vulis (1989), the surface albedo is not a surface property, nor can it easily be evaluated from satellite measurements.
- The demonstrated difficulties concerning narrowband-to-broadband conversion of surface albedos apply equally to surface SW fluxes. This raises an important issue concerning the use of narrowband measurements to determine surface SW radiation. It is problematical if such measurements, at least for vegetated surfaces, will ever prove to be useful for determining surface SW absorption, even if they were to prove useful with respect to surface insolation evaluations. The use of broadband measurements, such as those provided by the ERBE, eliminates this very difficult narrowband-to-broadband issue.
- The present study has demonstrated the usefulness of the BAO Tower measurements for validating one proposed means of transferring, for clear-sky conditions, broadband SW measurements from the TOA to the surface; it would obviously be advantageous to have additional measurements for other geographical domains.

Acknowledgments. The Boulder aerosol optical depth data were supplied by Pat Reddy. Don Nelson assisted in the operation and calibration of the tower instruments. This work was partially supported by NASA Contract NAS118155 and NSF Grant ATM-8815885 to SUNY Stony Brook.

REFERENCES

Bowker, D. E., R. E. Davis, D. L. Myrick, K. Stacy and W. T. Jones, 1985: Spectral reflectances of natural targets for use in remote sensing studies. NASA Ref. Publ. 1139, 181 pp. [Available from National Aeronautics and Space Administration, Code NIT-4, Washington, D.C. 20546-0001.]

Briegleb, B. P., P. Minnis, V. Ramanathan and E. Harrison, 1986: Comparison of regional clear-sky albedos inferred from satellite observations and model computation. *J. Climate Appl. Meteor.*, **25,** 214–226.

Cess, R. D., and I. L. Vulis, 1989: Inferring surface-solar absorption from broadband satellite measurements. *J. Climate,* **2,** 974–985.

——, G. L. Potter, J. P. Blanchet, G. J. Boer, S. J. Ghan, J. T. Kiehl, H. Le Treut, Z.-X. Li, X.-Z. Liang, J. F. B. Mitchell, J.-J. Morcrette, D. A. Randall, M. R. Riches, E. Roeckner, U. Schlese, A. Slingo, K. E. Taylor, W. M. Washington, R. T. Wetherald and I. Yagai, 1989: Interpretation of cloud-climate feedback as produced by 14 atmospheric general circulation models. *Science,* **245,** 513–516.

Chen, T. S., and G. Ohring, 1984: On the relationship between clear-sky planetary and surface albedos. *J. Atmos. Sci.,* **41,** 156–158.

d'Almeida, G. A., 1987: On the variability of desert aerosol radiative characteristics. *J. Geophys. Res.,* **92,** 3017–3026.

Deepak, A., and H. E. Gerber, 1983: Report on the experts meeting on aerosols and their climatic effects. World Climate Research Programme Rep. WCP-55, 107 pp.

ERBE Science Team, 1986: First data from the Earth Radiation Budget Experiment (ERBE). *Bull. Amer. Meteor. Soc.,* **67,** 818–824.

Gutman, G., G. Ohring, D. Tarpley and R. Ambroziak, 1989: Albedo of the United States Great Plains as determined from NOAA-9 AVHRR data. *J. Climate,* **2,** 608–617.

Kaimal, J. C., and J. E. Gaynor, 1983: The Boulder Atmospheric Observatory. *J. Appl. Meteor.,* **22,** 863–880.

Kriebel, K. T., 1977: Reflection properties of vegetated surfaces: Tables of measured spectral biconical reflectance factors. Wiss. Mitt. Nr. 29, Munchner Universitatsschriften, Meteorologisches Institut, Munchen, FRG, 82 pp.

Lacis, A. A., and J. E. Hansen, 1974: A parameterization for the absorption of solar radiation in the earth's atmosphere. *J. Atmos. Sci.,* **31,** 118–133.

McClatchey, R. A., R. W. Fenn, J. E. A. Selby, F. E. Volz and J. S. Garing, 1971: Optical properties of the atmosphere. Rep. AFCRL-71-0279, Air Force Cambridge Res. Lab., Cambridge, Mass., 85 pp.

Nack, M. L., and R. J. Curran, 1978: Transformation of surface albedo to surface-atmosphere albedo and irradiance and spectral and temporal averages. *Third Conference Atmospheric Radiation,* Amer. Meteor. Soc.

Pinker, R. T., 1985: Determination of surface albedo from satellites. *Adv. Space Res.,* **5,** 333–343.

Preuss, H. J., and F. Geleyn, 1980: Surface albedos derived from satellite data and their impact on forecast models. *Arch. Meteor. Bioklim.,* **A29,** 345–356.

Ramanathan, V., 1986: Scientific use of surface radiation budget data for climate studies. *Surface Radiation Budget for Climate Studies,* J. T. Suttles and G. Ohring, Eds., NASA Ref. Publ. 1169, 132 pp.

——, R. D. Cess, E. F. Harrison, P. Minnis, B. R. Barkstrom, E. Ahmad and D. Hartmann, 1989: Cloud-radiative forcing and climate: Results from the Earth Radiation Budget Experiment. *Science,* **243,** 57–63.

Reynolds, D. W., T. B. McKee and K. S. Danielson, 1978: Effects of cloud size and cloud particles on satellite-observed reflected brightness. *J. Atmos. Sci.,* **35,** 160–164.

Rossow, W. B., E. Kinsella, A. Wolf and L. Garder, 1987: International Satellite Cloud Climatology Project (ISCCP) description of reduced resolution radiance data. World Climate Research Programme Report WMO/TD-No. 58, 143 pp.

Schmetz, J., 1989: Surface radiation climatology: Retrieval of downward irradiances from satellites. *IRS '88: Current Problems in Atmospheric Radiation.* J. Lenoble and J.-F. Geleyn, Eds., A. Deepak, 653 pp.

Sellers, P. J., S. I. Rasool and H.-J. Bolle, 1988: Satellite data algorithms for studies of the land surface. International Satellite Land Surface Climatology Project (ISLSCP) Rep. No. 9, 140 pp.

Somerville, R. C. J., P. H. Stone, M. Halem, J. E. Hansen, J. S. Hogan, L. M. Druyan, G. Russell, A. A. Lacis, W. J. Quirk and J. Tenenbaum, 1974: The GISS model of the global atmosphere. *J. Atmos. Sci.,* **31,** 84–117.

Sparrow, E. M., and R. D. Cess, 1966: *Radiation Heat Transfer.* Brooks/Cole, 322 pp.

Vulis, I. L., and R. D. Cess, 1989: Interpretation of surface and planetary directional albedos for vegetated regions. *J. Climate,* **2,** 986–996.